Market Watch

Fab & Facilities

Materials

Cell Processing

Thin Film

PV Modules

Reducing the electrical and optical losses of PV modules incorporating PERC solar cells

Henning Schulte-Huxel, **Robert Witteck**, **Malte Ruben Vogt**, **Hendrik Holst**, **Susanne Blankemeyer**, **David Hinken**, **Till Brendemühl**, **Thorsten Dullweber**, **Karsten Bothe**, **Marc Köntges** & **Rolf Brendel**, Institute for Solar Energy Research Hamelin (ISFH), Emmerthal, Germany

ABSTRACT

The continual increase in cell efficiency of passivated emitter and rear cells (PERCs), as well as the optimization of the module processes, has led to significant advances in module power and efficiency. To achieve the highest module power output, one important aspect to consider is the optimization of the solar cell front metallization and the cell interconnection. An experimentally verified analytical model is used in combination with ray-tracing simulations to study the electrical and optical impact of the front-side metallization of the solar cells, as well as various configurations of the cell interconnector ribbons (including their cross section, number and optical properties), on the module power output. On the basis of the simulation results, a standard 60-cell module is processed with 120 halved PERCs, resulting in an independently confirmed power output of 303.2W and an efficiency of 20.2% on the aperture area. The module performance is analysed with reference to ISFH's optical and electrical simulations: the power loss due to the series interconnection of the solar cells is determined to be 1.5%. This power loss, however, is offset by a gain in current of 1.8% as a result of the change in the optical environment of the cells in a module as compared to in air.

Introduction

Passivated emitter and rear cells (PERCs) fabricated from p-type crystalline Si wafers are the cell technology with the largest predicted gain in market share in the future [1]. The efficiency of screen-printed industrial PERC solar cells has increased over the past few years, reaching record cell efficiencies of 22% [2,3].

Additionally, significant improvements have been made for a standard 60-cell module incorporating PERC solar cells. The highest reported and independently confirmed module efficiency so far has been 19.5% for a module with an output power of 294W [4]. Since that was published, new results have been documented regarding higher module powers; the current power record is 335.2W [5]. However, power-optimized modules often employ a larger module area in order to benefit from additional light collection from the regions between the cells; consequently, the 335.2W module has an efficiency of only 19.1% [5]. Increasing the module area, however, leads to an increase in material consumption, which in turn results in increased system costs [6].

To achieve the highest module efficiencies, the impacts of the relevant module components, as well as the effects of the adaptation of the cell properties for operation in the optical environment in the laminated module, are analysed in this paper. The focus is therefore on the screen-printing design, the configurations of the cell interconnector ribbons (including their cross section, number and optical properties), the impact of light-guiding structures between the cells, and the use of an encapsulant with enhanced UV transparency. For the resistive and electronic (recombination) effects, an analytical model is used [7]. Ray-tracing simulations [8] are employed to characterize the optical impact of structured ribbons [9], the cell metallization, the cell gap, the encapsulant, and the front glass on the module power output.

On the basis of the optimizations, a large-area 60-cell equivalent module was constructed from 120 halved 6" PERC cells with an average efficiency of 20.8%. A module power of 303.2W was obtained on an aperture area of 1.50m² (1,592mm × 943mm); this power corresponds to an efficiency of 20.2%. To the best of the authors' knowledge, this is the highest efficiency for a standard 60-cell module based on screen-printed p-type PERC silicon solar cells. The cell-to-module losses were analysed by sequentially including the following: the electrical losses due to the current mismatch effect, the resistive losses caused by the series interconnection of cells, and the optical gains and losses.

Optimization of cell front-side metallization and interconnections

Influence of the front metal fingers and cell interconnection ribbons

The influence of the number of front metal fingers and the cell interconnection on the module power output is simulated by means of a model presented in Witteck et al. [7]. The simulation parameters are taken from the same reference. For ISFH's simulations, a solar module consisting of 60 full and 2mm equally spaced PERC solar cells is used. The cell interconnection is realized by cell interconnection ribbons (CIRs) with a light-recovery probability k_{cir} of 0.1. (A k_{cir} of 0.1 means that 10% of the light that hits the CIRs is collected by the solar cells.) The thickness of the CIRs is limited in all simulations to 200μm in order to reduce any mechanical stresses that might induce cell cracking.

Fig. 1 shows the power output of a module for different numbers of CIRs and various CIR widths w_{cir}. In solar module factories, cell interconnection tools with up to five CIRs are implemented nowadays. On the assumption that there will be further advances in technology in the coming years, up to seven CIRs are considered in the simulations. The CIR width w_{cir} is varied between 0.6 and 2.5mm. (Smaller values for w_{cir} are not investigated,

as the current stringer technology is limited because of positioning accuracy.) For each number of CIRs, the number of front metal fingers (n_f) of constant width are optimized with respect to a maximum module power output. The value of n_f that results in the highest module power output for a specific number of CIRs is indicated in Fig. 1.

An increase in module power is observed for a decrease in w_{cir} from 2.5 to 0.6mm with increasing number of CIRs. However, for the cell configuration used, four to seven busbars give rise to similar module powers of 287.2±0.4W. The decrease in optimal CIR width results from the trade-off between the shading of the front side by the CIRs and the resistive power losses. If the CIR width becomes too wide, the shadow losses dominate and cause a decrease in power output.
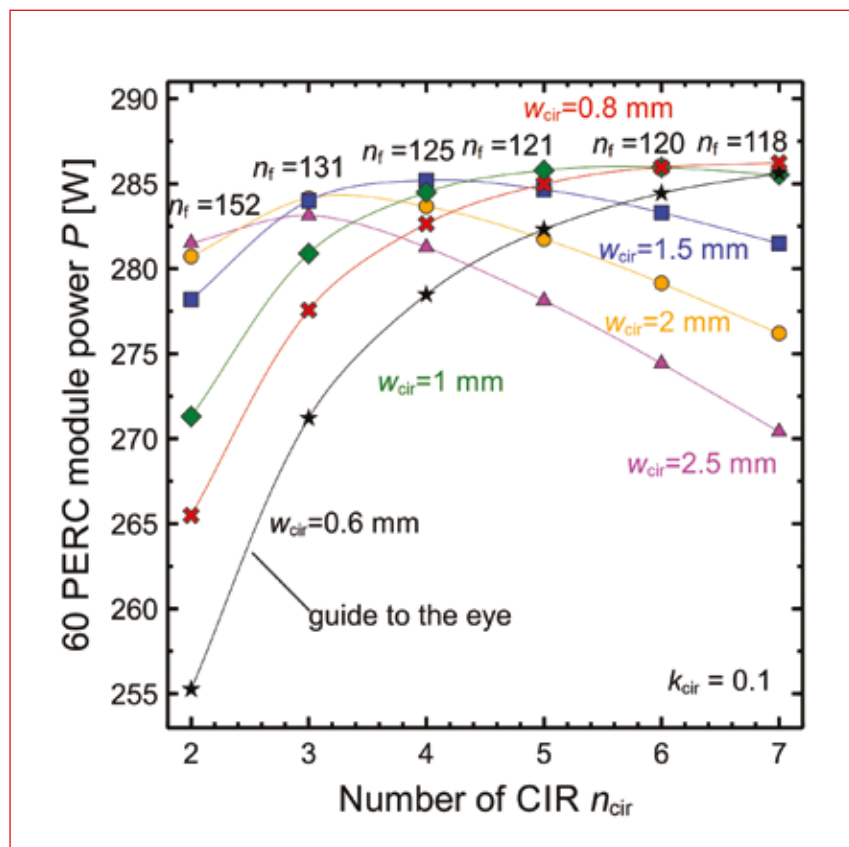
Figure 1. Simulated power output of a 60-PERC module for different numbers of CIRs per solar cell. Various CIR widths are considered for the simulation. The number of fingers is optimized for maximum module power output. For the simulation, full pseudo-square cells with standard CIRs and a $k_{cir} = 0.1$ are assumed.

> **"The optimal number of CIRs must be evaluated individually for each process line and cell design."**

Increasing the number of CIRs reduces the current path in the front metal fingers, and thus further reduces the series resistance losses, leading to the possibility of reducing the number of fingers. This has an impact on silver paste consumption, which is also affected by the increasing number of CIRs, demanding more, but narrower, screen-printed busbars. Moreover, the alignment of the CIRs is more challenging and the positioning accuracy of the stringer becomes crucial. The stringing machine also becomes more complicated, and more tools to produce the ribbons are required per watt peak when more CIRs are used. On the other hand, increasing the number of CIRs improves module reliability, as well as making the module power output more robust against cracks [10]. Consequently, the optimal number of CIRs must be evaluated individually for each process line and cell design.

Reducing electrical and optical losses of cell interconnection ribbons
Reducing the series resistance losses while limiting the shading of the cell by the CIRs is achieved by enhancing the optical properties of the CIRs. Within a module, light reflected by the CIRs may be totally internally reflected at the glass–air interface, and thus contribute to the generated cell current; this effect will reduce the effective optical width $w_{cir,eff}$ of the CIRs, which is taken into account by the light-recovery probability k_{cir}. Another possibility is to reduce the generated current of the cell by employing half-size cells.

Fig. 2 shows the schematics of the four state-of-the-art cell interconnection configurations modelled in the work reported in this paper. For configuration (a), standard CIRs with $k_{cir} = 0.1$ and full-size cells are considered. Configuration (b) uses the same CIRs, but only half cells; note that in this case, the module consists of 120 such cells. In
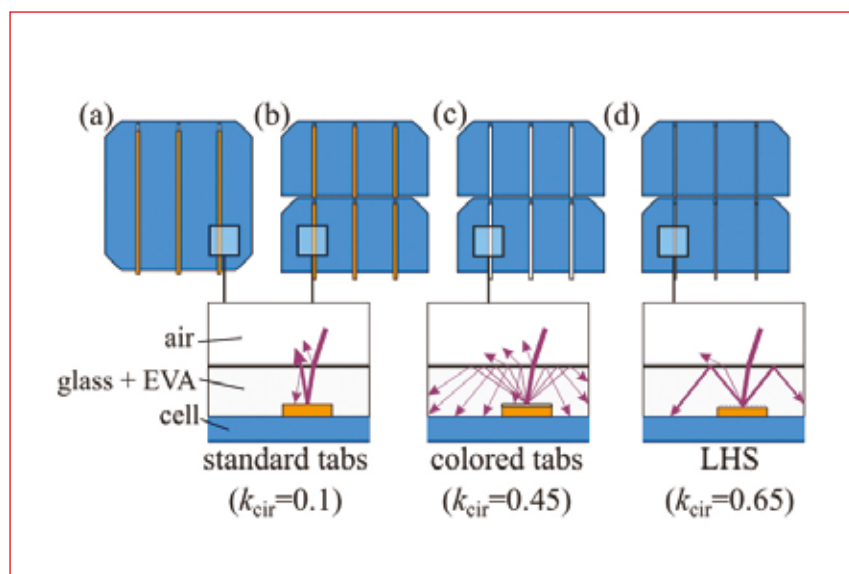

Figure 2. Solar cell interconnection configurations: (a) full cell with standard CIRs; (b) half cell with standard CIRs; (c) half cell with white CIRs; (d) half cell with structured CIRs. The insets show schematically the light scattering of the interconnection in a module. The k values denote the associated effective optical reduction ratios.

configuration (c), half cells with optically enhanced white CIRs, with $k_{cir} = 0.45$, are used [11].

For configuration (d), a structured light-harvesting string (LHS) ribbon (by Schlenk AG) is applied to the cells. Because of the structure, light impinging on the ribbon is reflected at a particular angle which increases the probability that it becomes totally internally reflected. Thus, the light-recovery probability reaches 0.65 to 0.75 [7,9]. As a conservative approximation, $k_{cir} = 0.65$ is used here.

Fig. 3 shows the simulated module power for configurations (a) through (d), for different numbers of CIRs. For each simulation, the width of the CIRs, w_{cir}, and the number of front metal fingers, n_f, are optimized for maximum module power.

In the simulations a maximum power output of approximately 286W for module (a), with full cells and $k_{cir} = 0.1$ (black curve in Fig. 3), is realized with seven CIRs of width 0.8mm. When the same number of CIRs is used, but the module current is reduced by 50% (i.e. employing half cells, (b), red curve), the module power increases by 6W. An improvement of the optics of the CIRs gains an additional 3.5W with the application of white CIRs ($k_{cir} = 0.45$, (c), green curve), and 6W with the application of structured CIRs ($k_{cir} = 0.65$, (d), blue curve).

In the case of $k_{cir} = 0.1$ and half cells, the optimum number of CIRs is six, while this figure shifts to seven if the effective optical width of the CIR is reduced. In contrast, the optimal width of the CIR increases from 0.8mm for the standard CIR ($k_{cir} = 0.1$), to 1mm for an optically enhanced CIR. However, the gain in module power seen through comparing 5, 6 or 7 CIRs for configurations (b) through (d) is approximately 1W.

When determining the optimal number of CIRs, it is crucial to take into consideration the additional costs of manufacturing tools, as well as the trade-off between fewer fingers and more busbars. Therefore, the practical optimum, depending on the tools used, can differ from the particular configuration that leads to the highest module power. Note that the cell gap is very small and that an enhanced internal reflection of light by the backsheet will increase the module current generated, resulting in more numerous and wider CIRs.

Furthermore, the use of half cells has some advantages and disadvantages. Some authors [5,12] state that there might be a larger impact due to cell mismatch from using half cells and thus twice as many cells; however, the use
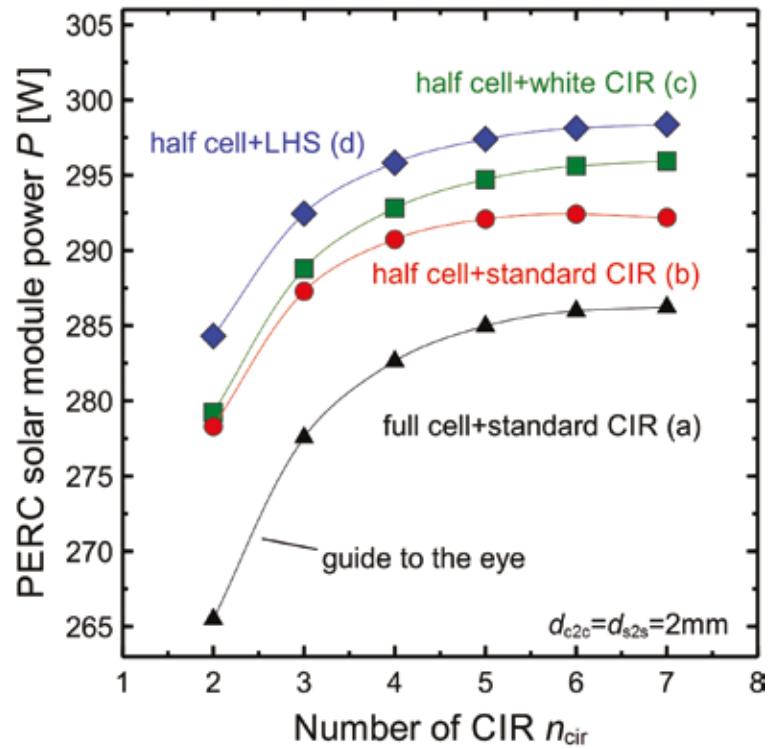
Figure 3. Simulated module power output for module configurations (a) through (d), with different numbers of CIRs. The cell gap is 2mm in all directions, and the number of front metal fingers is optimized for maximum module power output.
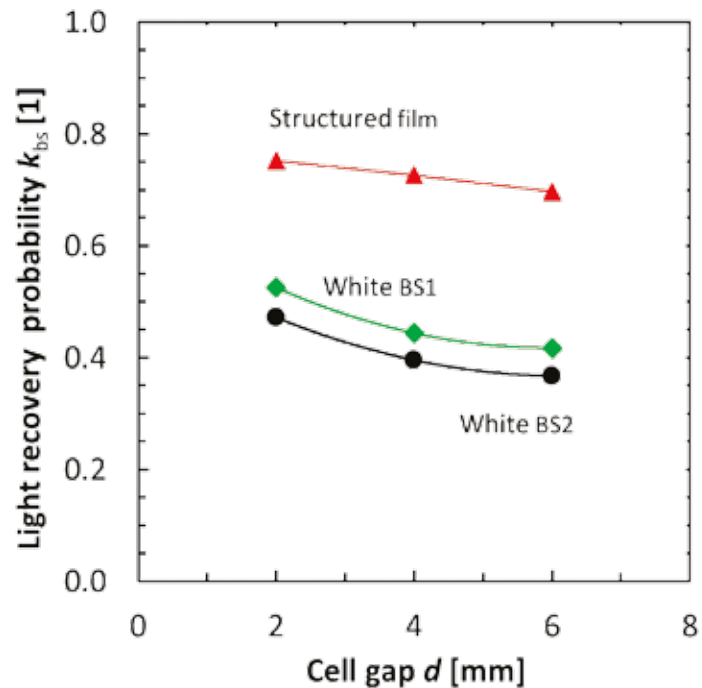

Figure 4. Experimentally determined light-recovery probabilities k_{bs} for various backsheets as a function of the cell gap d [17].

of cells that have been sorted (which is usually carried out by the cell producers) does not lead to a significant mismatch loss [13,14]. The yield and efficiency loss [12,15] caused by the laser-cutting step may be reduced by adapting the laser parameters, and in some cases an improved cell performance is even observed after the cutting process [16]. A disadvantage of using half cells is that the throughput of the stringer is halved with respect to the watt peak.

Optical properties of the cell and module components

Within a PV module, the current generation is affected by the parasitic absorption of photons by module components (i.e. the glass and encapsulation) in addition to absorption by the Si. Moreover, the reflection of incident light leads to optical losses, such as the reflection at the air–glass interface for incoming light. However, reflections also result in gains – for example, light reflected at the backsheet and back onto the cell surfaces as a result of total reflection at the glass–air interface.

In a first step, the experimental results are discussed, with a comparison of the optical performance of various backsheets (BSs). In a second step, the distribution of the light between all module components is considered.

Light recovery from the cell gaps

The light-recovery probability of the cell gaps/backsheet is defined as the portion of light collected by the solar cells that is reflected from the backsheet between the cells [17]. Fig. 4 shows the measurements of the light-recovery probabilities k_{bs} for various backsheets. Generally, white backsheets exhibit recovery factors of approximately 50%, which decreases with increasing cell gap d. Two white backsheets are shown in Fig. 4, which are representative of the range of seven tested commercially available backsheets. The collection of light hitting between the solar cells can be further improved by using structured and metallized films between the solar cells, yielding a k_{bs} of 75% (see Fig. 4).

Light distribution in a standard module vs. an optimized module

The DAIDALOS ray-tracing framework [8] is used, which employs a multi-domain approach [18]. This allows the simulation of entire solar modules in three dimensions, while also taking into account the front metallization, the inter-cell gaps, and the large number of pyramids of the textured silicon

surface in excess of 10^{10}. Additionally, a collection efficiency specifically simulated using Sentaurus is employed to match the properties of the cells in order to differentiate between photogenerated and short-circuit current.

With this combination of tools, there is good agreement between simulated and measured module J_{sc} [19]. The profiles and properties of the fingers and CIRs are given in Witteck et al. [11] and Holst et al. [9] respectively. The thicknesses of the dielectric layers and Lambertian factor of the rear side are determined from reflection measurements. The complex refractive index data for low iron soda lime glass are taken from Volgt et al. [20], and the encapsulation material data are found in Vogt et al. [19]. The properties of the other material data for the module components and their measurements are given in Vogt [21].

Fig. 5 shows the percentage of incoming light that is converted into short-circuit current or lost for a standard module with full-size PERC cells and the high-efficiency PERC module; data are given for wavelengths between 300 and 1,200nm in 10nm steps. For the high-efficiency module, three optical improvements are considered:

1. The use of light-harvesting structures in the cell gap instead of a white backsheet: this decreases the absorption in the cell gap (light green), and reduces reflection (dark green).

2. The replacement of standard CIRs by interconnections with light-harvesting structures: this decreases the absorption in the front metal (red), and reduces reflection (dark green).

3. The replacement of conventional ethylene-vinyl acetate (EVA) by EVA with enhanced UV transmission: this decreases the absorption in the encapsulation (blue), which has demonstrated a 1.4% improvement in module short-circuit current with similar cells [19].

> **"The use of light-harvesting structures in the cell gap instead of a white backsheet decreases the absorption in the cell gaps and reduces reflection."**

Regarding the remaining losses in the high-efficiency module, the largest absorption contribution in the infrared range originates from the cell rear-side metallization, where the Si absorption coefficient decreases [22]. In the UV wavelength region, the limiting factor is the parasitic absorption in the glass, which can be reduced by further eliminating the concentration of the Fe^{3+} ions in the glass [20]. In contrast, reflection losses are the main limiting factor in the visible wavelengths.

Fabrication of a high-efficiency module

To demonstrate the application of the above-mentioned improvements, a module consisting of 120 half cells was constructed. The PERC solar cells were processed in the SolarTeC technology centre using industrial production tools, similarly to Hannebauer et al. [23]. The front-side metallization was adapted to a half-cell design, and the number of fingers was optimized for the operating environment within the laminated module [11]. The cells feature four 1mm-wide busbars, which represents a trade-off between reducing the power loss and the number of solder steps, since the cells are interconnected manually.

The half cells are interconnected by LHS ribbons having a cross section of $0.2 \times 1.5mm^2$. Six strings, each consisting of 20 half PERC cells, are connected in series using string interconnection ribbons (SIRs) with a cross section of $0.2 \times 6mm^2$. In order to reduce the module area, a distance d_{s2s} (string-to-string gap) of 1mm between adjacent strings was used, together with a distance d_{c2c} (cell-to-cell gap) of 1.5mm between the solar cells within a string. Compared with the aperture area of a module with pseudo-square cells and a cell gap of 2mm, the total module size is reduced by 2.6%. More importantly, the area fraction covered by the solar cells, or the aperture module area, is increased from 93% to more than 97%.

The trapping of the light hitting the remaining cell gaps is increased by a structured and metallized foil as described earlier. The cell matrix is laminated with EVA (450µm thick, EVASKY S87, Bridgestone), a 3.2mm-thick front glass with an anti-reflection coating (f|solarfloat HT by f|solar), and a white backsheet (PYE 3000, Coveme). Fig. 6 shows a photograph of the front side of the framed module.

Cell-to-module loss analysis

The characteristic $I–V$ parameters of the 120 cells are measured before interconnection and lamination; these are listed in Table 1, row A. To avoid a mismatch of the cell currents, the impact of the mismatch on module performance is analysed by interpolating the individual light $I–V$ characteristics of the cells, and by summing the voltages of the 120 cells for each current value. The parameters of the $I–V$ characteristic obtained for the module in the case of a loss-free interconnection are given in row B. Comparing rows A and B shows that the impact on the short-circuit current I_{sc} due to the mismatch is small ($0.01A$ or $0.3\%_{rel}$), and is offset by an increase in the fill factor FF. As the open-circuit voltage V_{oc} is unaffected by the mismatch, the power of the 120 cells is unchanged.

Row C of Table 1 includes the series resistance contribution of the CIRs (on and between the solar cells) and the SIRs (between the strings and to the external module contacts). The series resistance contribution due to the cell interconnection by the CIRs and SIRs is analytically determined to be
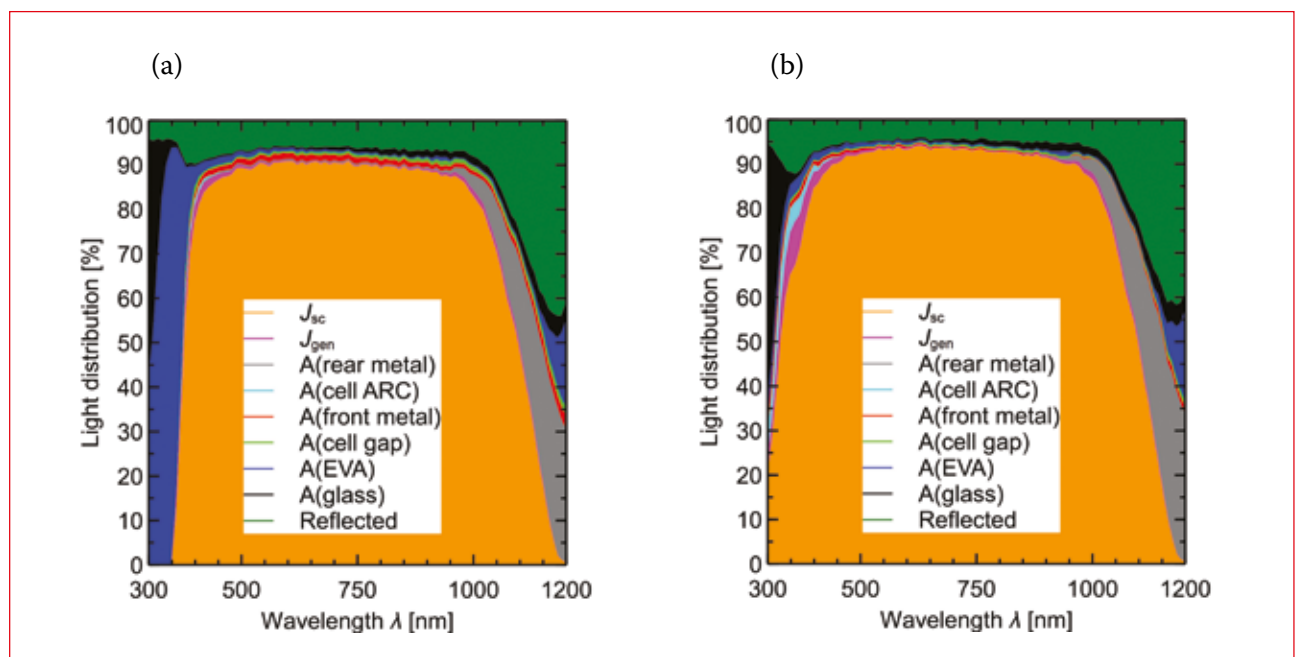

Figure 5. Optical loss analysis under normal incident light: (a) standard module; (b) high-efficiency PERC module.

$0.14\Omega cm^2$ and $0.08\Omega cm^2$ respectively. These resistances decrease the fill factor by $0.9\%_{abs}$ ($1.1\%_{rel}$) compared with the average of the initial cells; this corresponds to a fill factor of 78.7% and results in a power loss of 4W. Besides electrical losses, there are also optical effects, which are determined using ray-tracing simulation.

Fig. 7 shows the current losses, which are determined by multiplying the photocurrent distribution (as in Fig. 5) with the AM1.5G spectrum, and then integrating over all wavelengths. A light ray contributes to the reflection losses of an interface if the ray reaches that interface but never passes it, and if that ray additionally leaves the module. Here, a cell before module integration, with a short-circuit current of 4.79±0.002A (numerical uncertainty of the Monte-Carlo algorithm of the ray-tracing simulations), is simulated. The simulations show good agreement with the experimentally measured half PERC cells, which yielded a short-circuit current of 4.80±0.08A (uncertainty of the cell measurements).

A comparison of the cell before and after module integration reveals that the changes in absorption losses in the Al rear metallization and the cell anti-reflection coating (ARC) are not significant. Even though the CIRs are wider and longer than the busbars, the absorption by the front metal only increases from 0.02 to 0.03A; in the case

Figure 6. Photograph of the ISFH high-efficiency module, consisting of 120 half PERC solar cells.

of standard CIRs this effect is greater, but because of the structure of the CIRs in ISFH's module [9], this loss factor is reduced.

The reflection at the cell ARC is reduced by a factor of two because of the higher reflection index of EVA compared with air. As a result of internal reflections, the reflection losses relating to the fingers and the busbars/CIRs are reduced by 63% and 74% respectively, compared with the

Row		I_{sc} [A]	V_{oc} [V]	FF [%]	P_{mpp} [W]	η [%]
A	Measurements of 120 half cells	4.80[†]	79.4[§]	79.6[†]	303[§]	20.8[†]
B	Simulation of mismatch effect	4.79	79.4	79.9	303	
C	Simulation of interconnected cells (resistive effects)	4.79	79.4	78.7	299	
D	Simulated module (incl. elec. and opt. effects)	4.87	79.4	78.7	304	
E	Measured module[#]	4.86[*]	79.1[*]	78.9[*]	303[*]	20.2

[§] Sum over all cells.
[†] Average of all cells.
[#] Module measurements on aperture area (ap.) (excluding frame).
[*] Independently confirmed by TÜV Rheinland, Cologne, Germany.

Table 1. Measurements and simulations of the characteristic $I–V$ parameters of the interconnected cells and the module under standard testing conditions (AM1.5G, 100mW/cm^2, 25°C). The solar cells each have an area of 121.67cm^2, and the module has an aperture area of 15,008cm^2.
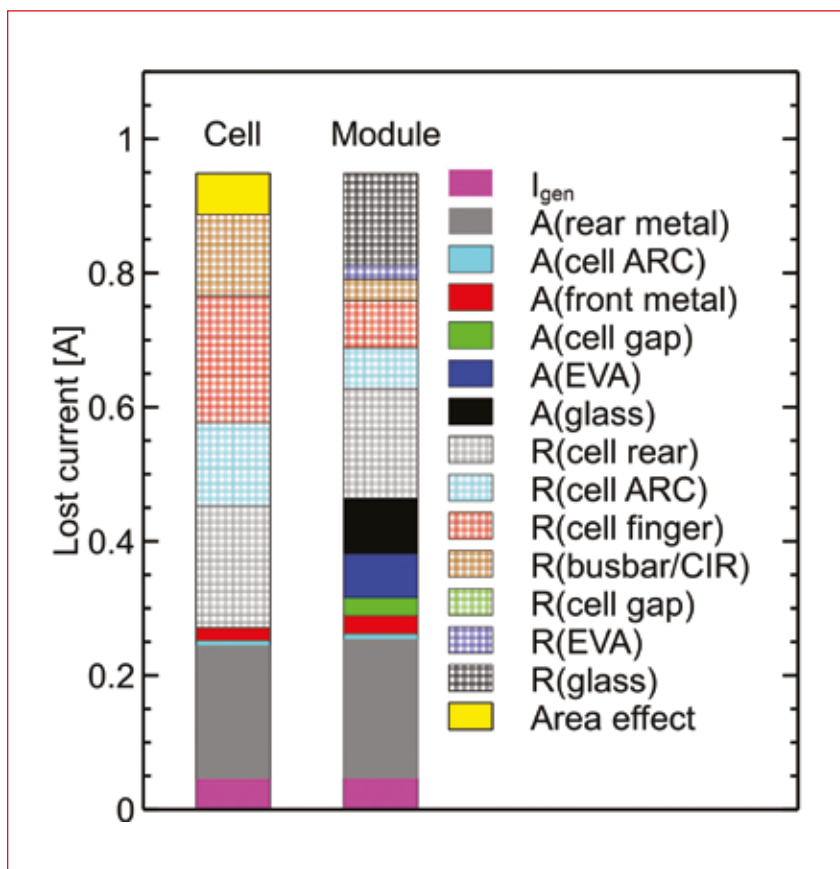
Figure 7. Comparison of the simulated electrical current and optical losses for the cell before and after module integration under normal incident light and AM1.5G spectrum. Only light which leaves the module as reflected light is considered. Since the cell in air collects light on a smaller area (cell area) compared with the cell in the laminate (cell area + cell gap), this area effect is included in the comparison.

cell before lamination. This underlines the importance of optimizing the cell metallization with respect to the operational environment within the laminate. In the module, additional absorption takes place in the glass, the EVA and the cell gap, and there are reflection losses at the air–glass and glass–EVA interfaces. Since the cell before module integration collects light on a smaller area (cell area) compared with the cell in the laminate (cell area + cell gap), this area effect is included in the comparison.

The module simulations yield a short-circuit current of 4.88A, which corresponds to a cell-to-module I_{sc} gain of 1.8%. This cell-to-module gain is included in the calculation results in row D of Table 1, which shows an I_{sc} of 4.87A and a module power of 304W; this is in good agreement with the module measurements of 303W determined independently by TÜV Rheinland, as shown in row E of the table.

Conclusion

The effects of various adaptations of the module process, as well as their impact on module performance, have been presented. Several aspects were analysed and discussed, especially the number and properties of CIRs, the usage of half cells, and the impact of enhanced optical properties of the CIRs and in the cell gaps. Half cells and structured CIRs increase the module power to 297W, compared with 285W for full cells and conventional ribbons, when using five-busbar solar cells. Increasing the number of busbars, however, has only a small impact on module performance.

It was also shown that the module current can be significantly increased by using metallized and structured materials in the cell gaps and on the ribbons, where the light recovery can be enhanced by 50% and 700% respectively.

With the described adaptations of the module, a best technical practice module was constructed with 120 half PERC solar cells; this yielded a module efficiency of 20.2%. No power loss due to cell mismatch was found. The interconnection of the cells by the CIRs, and of the strings by the SIRs, results in a decrease in FF of 0.9%$_{abs}$ compared with the average FF of the cells, and in a power loss of 4W. The optical behaviour of the module was simulated by ray tracing. It was shown that, because of a net cell-to-module gain in current of 1.8%, the final simulated module achieves a module power output of 304W; compared with the 303W obtained from the independently confirmed module measurements, this demonstrates the predictive strength of ISFH's model.

"The presented module achieves a record efficiency of 20.2% for a standard 60-cell PERC module."

The ray-tracing simulations showed that a large absorption loss originates from the cell's rear-side metallization. This loss can be reduced, for example, by using bifacial PERC+ or PERT cells, as shown in Dullweber et al. [24]; cells of this type would be also be beneficial in monofacial modules, such as the module investigated here.

In order to reduce the cell-to-module losses in efficiency, the total module area was decreased, and the fraction of the active module area (solar cells) was increased: the aperture area was reduced by 2.6% compared with a standard module, and the active area was increased to more than 97%. With this increase in active cell area, combined with a minimization of the power losses within the module, the presented module achieves a record efficiency of 20.2% for a standard 60-cell PERC module. To the best of the authors' knowledge this is the highest efficiency for a standard 60-cell module based on screen-printed p-type PERC silicon solar cells.

By virtue of their consuming less construction and cabling material, high-efficiency modules using industrially processed screen-printed p-type PERC silicon solar cells are particularly relevant to further reducing the balance of system costs, and thus the levelized cost of PV-generated electricity.

References

[1] SEMI PV Group Europe 2016, "International technology roadmap for photovoltaic (ITRPV): 2015 results", 7th edn (Mar.) [http://www.itrpv.net/Reports/Downloads/].

[2] SolarWorld 2016, Press Release (Jan.) [http://www.solarworld.de/konzern/presse/aktuelles/pressemitteilungen/single-pressemitteilung/article/solarworld-praesentiert-solartechnik-der-naechsten-generation/].

[3] Ye, F. et al. 2016, "22.13% efficient industrial p-type mono PERC solar cell", *Proc. 43rd IEEE PVSC*, Portland, Oregon, USA.

[4] Metz, A. et al. 2014, "Industrial high performance crystalline silicon solar cells and modules based on rear surface passivation technology", *Sol. Energy Mater. Sol. Cells*, Vol. 120, pp. 417–425.

[5] Zhang, S. et al. 2016, "335-W world-record p-type monocrystalline module with 20.6% efficient PERC solar cells", *IEEE J. Photovolt.*, Vol. 6, No. 1, pp. 145–152.

[6] Verlinden, P. et al. 2013, "Cost analysis of current PV production and strategy for future silicon PV modules", *Proc. 28th EU PVSEC*, Paris, France.

[7] Witteck, R. et al. 2016, "Optimized interconnection of passivated emitter and rear cells by experimentally verified modeling", *IEEE J. Photovolt.*, Vol. 6, No. 2, pp. 432–439.

[8] Holst, H. et al. 2013, "Application of a new ray tracing framework to the analysis of extended regions in Si solar cell modules", *Energy Procedia*, Vol. 38, pp. 86–93.

[9] Holst, H. et al. 2016, "Increased light harvesting by structured cell interconnection ribbons: An optical ray tracing study using a realistic daylight model", *Energy Procedia* [forthcoming].

[10] Gabor, A.M. et al. 2015, "Solar panel design factors to reduce the impact of cracked cells and the tendency for crack propagation", *Proc. NREL PV Mod. Rel. Worksh.*, Golden, Colorado, USA.

[11] Witteck, R. et al., "Optimizing the solar cell front side metallization and the cell interconnection for high module power output", *Energy Procedia* [forthcoming].

[12] Pan, X. et al. 2014, "Theoretical and experimental study of power loss in half-cell PV modules", *Proc. 8th SNEC Int. PV Power Gen. Conf.*, Shanghai, China.

[13] Evans, R. et al. 2015, "Simplified technique for calculating mismatch loss in mass production", *Sol. Energy Mater. Sol. Cells*, Vol. 134, pp. 236–243.

[14] Schulte-Huxel, H. et al. 2016, "High efficiency modules with passivated emitter and rear solar cells – An analysis of electrical and optical losses", Submitted for publication in *IEEE J. Photovolt.*

[15] Müller, J. et al. 2015, "Resistive power loss analysis of PV modules made from halved 15.6×15.6 cm^2 silicon PERC solar cells with efficiencies up to 20.0%", *IEEE J. Photovolt.*, Vol. 5, No. 1, pp. 189–194.

[16] Schulte-Huxel, H. et al. 2016, "Flip-flop cell interconnection enabled by an extremely high bifacial factor of screen-printed ion implanted n-PERT Si solar cells", *Proc. 32nd EU PVSEC*, Munich, Germany, pp. 407–412.

[17] Köntges, M. et al. 2016, "Method to measure light recovery probability of PV module backsheets enabling 20.2% module efficiency with passivated emitter and rear solar cells", *Proc. 32nd EU PVSEC*, Munich, Germany, pp. 1532–1538.
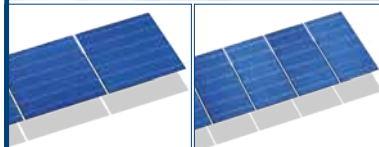
[18] Winter, M. et al. 2015, "Combining structures on different length scales in ray tracing: Analysis of optical losses in solar cell modules", *Opt. Quant. Electron.*, Vol. 47, No. 6, pp. 1373–1379.

[19] Vogt, M.R. et al. 2016, "Optical constants of UV transparent EVA and the impact on the PV module output power under realistic irradiation", *Energy Procedia* [forthcoming].

[20] Vogt, M.R. et al. 2016, "Measurement of the optical constants of soda-lime glasses in dependence of iron content and modeling of iron-related power losses in crystalline Si solar cell modules", *IEEE J. Photovolt.*, Vol. 6, No. 1, pp. 111–118.

[21] Vogt, M.R. 2015, "Development of physical models for the simulation of optical properties of solar cell modules", Ph.D. dissertation, Leibniz University Hannover.

[22] Schinke, C. et al. 2015, "Uncertainty analysis for the coefficient of band-to-band absorption of crystalline silicon", *AIP Adv.*, Vol. 5, No. 6, p. 67168.

[23] Hannebauer, H. et al. 2014, "21.2%-efficient fineline-printed PERC solar cell with 5 busbar front grid", *physica status solidi (RRL)*, Vol. 8, No. 8, pp. 675–679.

[24] Dullweber, T. et al. 2016, "BiCoRE: Combining a PERC-type cell process with n-type wafers", *Photovoltaics International*, 33rd edn.

About the Authors

Henning Schulte-Huxel studied in Leipzig, Germany, and in Bucharest, Romania, and received a master's in physics in 2010 from Leibniz Institute of Surface Modification, Leipzig. In 2015 he was awarded a Ph.D. for his work at ISFH on laser microspot welding for the interconnection of back-contacted silicon solar cells. Since 2014 he has been leading a project at ISFH that focuses on the module integration of PERC solar cells and the analysis and reduction of cell-to-module losses.

Robert Witteck studied renewable energies in Berlin. Since 2014 he has been at ISFH, working towards his Ph.D. on PERC module loss analysis.

Malte Ruben Vogt studied physics at the Leibniz University of Hanover, Germany, and received his bachelor's in 2009 and his master's in 2011. In 2015 he finished his Ph.D. at ISFH, where he worked on developing physical models for simulating the optical properties of solar cell modules. His current research focuses on the optical characterization of solar cell module components, and on the simulation of optical and thermal behaviour of PV modules in the field.

Hendrik Holst studied physics at the Leibniz University of Hanover, Germany. In 2015 he received his Ph.D. for work on the development of a modular ray-tracing framework and its application to multiscale simulations in PV. Since 2008 he has been with the simulation team at ISFH, where he is currently involved with optical simulations and optimization of solar cell modules.

Susanne Blankemeyer qualified as an optician at Krane-Optic in Rheda-Wiedenbrück in 1986, and worked as a laboratory assistant in the R&D department at Orbotech in Bad Pyrmont from 1999 to 2007. In 2007 she joined the module and interconnection technology group at ISFH, where she is currently working on the development of novel interconnection techniques and module concepts.

David Hinken studied physics at the University of Hanover, Germany, and the University of La Laguna, Spain. He received a Diploma degree in physics in 2007, and a Ph.D. in physics in 2012 for his work on luminescence-based characterization of crystalline silicon solar cells. He currently works in the solar cell characterization group and the calibration and test centre at ISFH.

Till Brendemühl received his Diploma degree in engineering physics from the University of Applied Science in Emden, Germany. Since 2005 he has been with ISFH, where he first worked on laser processes, later becoming project leader with a focus on back-contact high-efficiency solar cells. He currently works on screen-printed n-PERT and PERC solar cells in the future technologies photovoltaics group.

Dr. Thorsten Dullweber leads the industrial solar cells R&D group at ISFH. His research work focuses on high-efficiency, industrial-type, PERC silicon solar cells and on ultra-fine-line, screen-printed, Ag front contacts. Before joining ISFH in 2009, he worked for nine years as a project leader in the microelectronics industry at Siemens AG and then at Infineon Technologies AG.

Karsten Bothe received his Diploma degree in physics from the University of Oldenburg, Germany, after which he joined ISFH. He was awarded a Ph.D. in 2006 by the University of Hanover, Germany, for his work on oxygen-related trapping and recombination centres in boron-doped crystalline silicon. In 2007 he became head of the solar cell characterization group at the ISFH, where his current research interest is the calibrated measurement of the characteristic parameters of crystalline silicon solar cells.

Dr. Marc Köntges received his Ph.D. in physics in 2002 from the University of Oldenburg, Germany, for his research involving thin-film solar cells. He is head of the module technologies group at ISFH, where he currently works on the development of characterization and production methods for PV modules.

Rolf Brendel received a Ph.D. in materials science in 1992 from the University of Erlangen, Germany, for his work on infrared spectroscopy. After a research post at the Max Planck Institute for Solid State Research in Stuttgart, he was appointed head of the thermosensorics and photovoltaics division at the Bavarian Center for Applied Energy Research in 1997. In 2004 he joined the Institute of Solid State Physics at the Leibniz University of Hanover as a full professor, and became director of ISFH.

PV Modules